AIAA 80-0994R

Experimental Verification of Propeller Noise Prediction

George P. Succi,* David H. Munro,† and Jeffrey A. Zimmer‡
Massachusetts Institute of Technology, Cambridge, Massachusetts

An experimental study of the sound field of ¼-scale general aviation propellers has been completed. The results of these experiments, along with a comparison of the wake surveys and pressure signatures to the theoretical calculations, are presented. The calculations are both aerodynamic and acoustic. Given the airfoil section properties, the blade loading is calculated using a modified strip analysis procedure. The important contribution is the acoustic calculation. This is done by modeling the propeller as an array of point sources with each point characterized by the force and motion of the associated propeller section. Accurate results are obtained over a variety of operating conditions, tip speeds, and propeller nacelle combinations. No empirical adjustments are used. All calculations are made given only the shape and motion of the propeller.

Introduction

THE Massachusetts Institute of Technology has completed an experimental study of the sound field of ¼-scale general aviation propellers. Herein we present the results of the experiments along with a comparison of the experimental wake surveys and pressure signatures to theory. The calculations are both aerodynamic and acoustic. Given the airfoil section characteristics, the blade loading is calculated using a modified strip analysis procedure.[1] The propeller is then divided and modeled as an array of point sources with each point characterized by the force and volume of the corresponding propeller section.[2]

Three propellers were constructed:

Propeller 1—a scale model of a 1C160 propeller used to power a Cessna 172 Skyhawk, which we refer to as the production propeller.

Propeller 2—a scale model of a propeller with the radial loading moved inboard. At a given ratio it absorbs about 50% more power and produces about 50% more thrust than the production propeller.

Propeller 3—a scale model of a possible low propeller for a Cessna 172 Skyhawk. The propeller has power and thrust characteristics similar to propeller 1; however, it is designed to move the peak radial loading inboard.

Each propeller is a ¼-scale replica of the existing, or proposed, full-scale propeller. The propellers are mounted on a test stand in an anechoic wind tunnel. The test stand can be fitted with different aerodynamic fairings so as to explore the influence of the nacelle on the propeller (Fig. 1). Three fairings were constructed:

1) Minimum body—the smallest possible structure that covers the propeller drive motor.

2) Symmetric body—a large axially symmetric fairing with a meridian line chosen to approximate the axial cross area distribution of a typical light airplane fuselage.

3) Asymmetric body—a variation of the symmetric body wherein the upper portion of the body is modified to be a 2:1 axis ratio ellipse and then transformed into a conical "windshield" region, which is then faired into the round body.

The greatest effects are caused by a change in the propeller operating condition or observer location. Hence, for the most part, we discuss the production propeller operating in front of the symmetric body.

Presented as Paper 80-0994 at the AIAA 6th Aeroacoustics Conference, Hartford, Conn., June 4-6, 1980; submitted July 18, 1980; revision received Jan. 25, 1982.

*Research Associate, Dept. of Aeronautics and Astronautics; presently with Renault, Paris, France.

†Graduate Student, Dept. of Physics.

‡Hertz Fellow, Dept. of Mechanical Engineering.

Apparatus and Procedure

Apparatus

The propeller tests take place in the MIT anechoic wind tunnel (Fig. 2). This test section is an open jet, 2.3 m wide by 1.5 m high and 3.0 m long, surrounded by an anechoic room $6.8 \times 3.5 \times 3.5$ m. Room resonances are not important at frequencies above 160 Hz. Details of this tunnel are described in Ref. 3.

The major piece of equipment constructed for the experiment is the motor and support stand used to spin the propellers (Fig. 3). The stand is designed to spin ¼-scale general aviation propellers at full-scale tip speeds. The motor can spin up to 10,000 rpm and produce about 10 hp. Provision is made to measure thrust, torque, yaw, and propeller rpm. The angular position of the propeller is measured to 1% accuracy with an optical trigger.

The propeller blades are attached to the shaft via a hub, which allows the blades to be rotated to different angular positions. The blade angle is set by reflecting a laser beam off the pressure side of the propeller at the 80% radius. The blade twist is known to ¼-deg accuracy.

The microphone is located in the airstream to avoid refraction effects through the tunnel jet shear layer. A rectangular rack supports the ⅛-in. B&K microphone on adjustable boom. The rack can be rotated through an angle of ±42 deg with respect to the disk plane about a vertical axis passing through the propeller center. A balsa tail assembly keeps the microphone aligned with the local stream direction.

The microphone signal is amplified by a B&K model 2604 amplifier and recorded with an Explorer III digital oscilloscope. The oscilloscope can sample at a rate exceeding the direct memory access rates in conventional small computers. This aspect lets one take full advantage of the 80-kHz high frequency cutoff of the ⅛-in. microphone by sampling at rates exceeding 160 kHz.

Earlier calculations by Succi[2] demonstrated that the radial load distribution strongly influenced the resultant sound field. Propellers 2 and 3 are designed to have the peak-radial load more inboard than is normally the case. Wake surveys are made to deduce the blade loads. The survey is done with a motorized traverse that moves the probe radially through the slipstream, with a resolution of one part in 375.

Two probes are used for the wake measurements. The first is a three-hole pitot static pressure probe, which is called a cobra probe. The plane containing the three holes is tangent to

the cylinder centered on the propeller axis. By proper data reduction one can recover the static pressure, the flow velocity, and the swirl angle.[4,5]

A second set of measurements is performed with a hot wire anemometer. This anemometer is a 35-deg slanted single sensor hot wire whose support axis is mounted at approximately 10 deg to the propeller axis. The same motorized transverse is used with the hot wire mounted in place of the cobra probe. Four separate sweeps are made. Before each sweep the wire is rotated 90 deg about its support axis. Three positions are sufficient to span velocity space; the fourth is for redundancy.

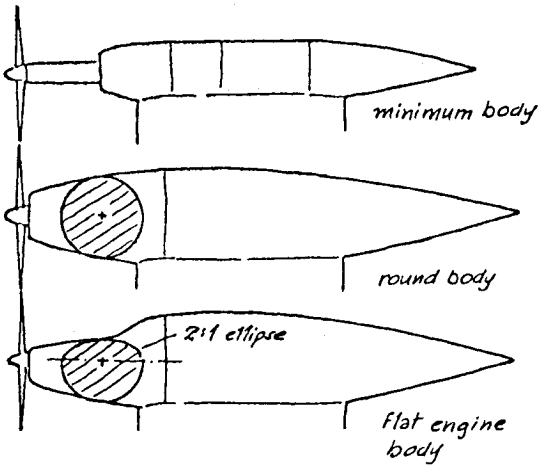

Fig. 1 Bodies tested with propellers.

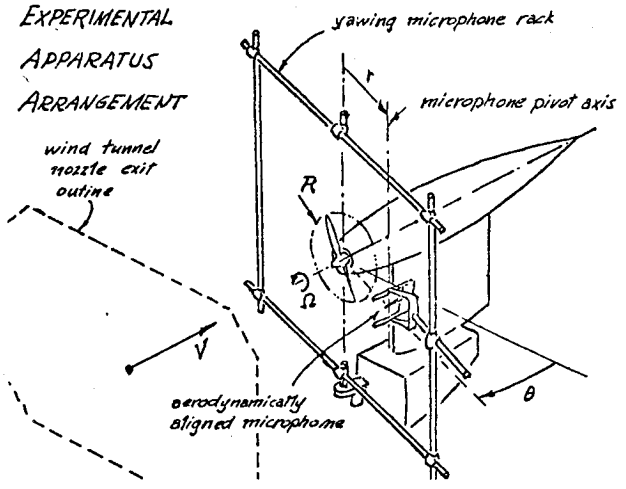

Fig. 2 Microphone rack.

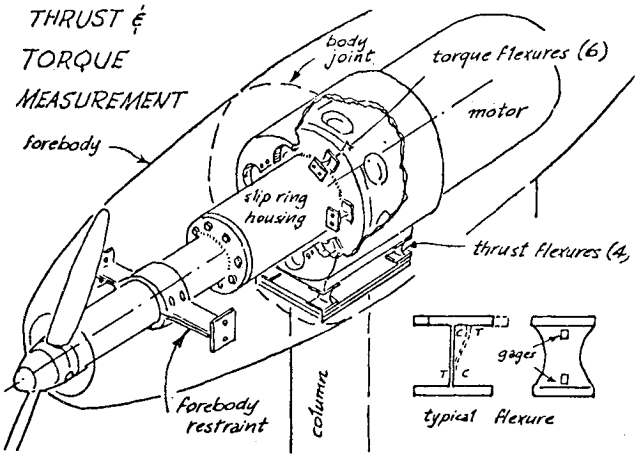

Fig. 3 Thrust stand.

Similarity Considerations

If two propellers are geometrically similar, there are three nondimensional numbers that must be fixed in order for model-scale measurements to compare to full-scale results. These are advance ratio, tip Mach number, and Reynolds number. The advance ratio ($\lambda = V/\Omega R$) is the ratio of forward velocity (V) to the tip speed (ΩR). This ratio sets the angle of attack at each radial station on the propeller. In the absence of compressibility and viscous effects, two propellers operating at the same advance ratio are aerodynamically similar in that their radial load distribution is identical.

The Mach number is most important in determining the sound field. Sound radiation from a propeller depends critically on the ratio of the tip speed to the speed of sound. To maintain Mach number similarity we spin the propeller four times as fast. If time is normalized to the shaft rotation period and distance to the propeller diameter, the pressure signature from a model propeller is identical to that for a full-scale propeller at the corresponding normalized point in space and time. The Mach number also influences the airfoil section characteristics. A rough rule is the Glauert law, which gives

$$\frac{dC_l}{d\alpha_M} = \frac{dC_l}{d\alpha_{M=0}} \frac{1}{\sqrt{1-M^2}} \tag{1}$$

where C_l is the section lift, α the angle of attack, and M the Mach number.

Given a similar advance ratio and Mach number, and faced with the practical constraint that the experiment is performed in room temperature air, it is impossible to keep the Reynolds number constant. In these experiments Reynolds number is always one-fourth the full-scale value. Airfoil section characteristics change somewhat with Reynolds number, thus breaking the similarity of our model test to a full-scale test. At 10,000 rpm the model-scale Reynolds number exceeded $0.25 + 10^6$ for radii outboard of the 25% station. At these Reynolds numbers the section characteristics approach their asymptotic values and the differences between model- and full-scale tests are small. At lower rpm, however, we expect viscous effects to play an increasingly important role in breaking the model/full-scale similarity.

Experimental Procedure

Two classes of experiments are discussed: propeller aerodynamics and propeller acoustics. The primary goal is to calculate the propeller sound field. However, accurate information about the blade loading is needed to do this correctly. A simple lifting line theory is used to develop the loading. Several experiments were devised to check the theory.

The first experiment is to measure the thrust and torque produced by the propeller at different rotation speeds and tunnel velocities. This permits a global check on the calculations and guarantees that the correct order of magnitude for the loads is obtained. The more refined check on the theory is to make a wake survey. Surveys are performed at three axial distances: 0.12, 0.50, and 1.23 radii. All surveys are done at a tunnel speed of 29 m/s and at two rotation speeds, 7000 and 10,000 rpm. The technique is discussed at length by Zimmer.[5]

For each propeller body combination three types of acoustic experiments are performed: an angular survey, a constant velocity survey, and a constant advance ratio survey. Each survey is a systematic perturbation about an operating point at 10,000 rpm and a tunnel speed of 29 m/s. This point corresponds to the takeoff condition (2500 rpm full scale and approximately 65 mph) for a Cessna 172 Skyhawk. It is

preferable to center data at a cruise operating point; however, the tunnel would not go faster than 30 m/s.

The angular survey is made with the propeller at 10,000 rpm and the tunnel velocity at 29 m/s. The microphone is located in the airstream about 0.49 m from the propeller center. The azimuthal position of the microphone was varied from −40 deg to +40 deg in 10-deg intervals. Angular measurements are made from the disk plane with angles upstream from the disk termed positive and those downstream termed negative.

The constant advance ratio surveys are made by holding constant the ratio of the tunnel speed to tip speed. Measurements are made at various tip speeds, with larger sampling at the higher speeds. Here the microphone is held in the disk plane. The point of the measurement is to explore the effect of tip Mach number at approximately identical radial loading. As noted before, the radial loads do change somewhat as a result of compressibility effects.

The constant velocity surveys are made by holding the tunnel speed constant (29 m/s) and varying the propeller tip speed. Again the microphone is held in the disk plane. As the tip speed drops, the radial loading changes. At the cruise advance ratio the propeller has a radial load pattern similar to the full-scale tests. Of course, since the Mach number is different, the sound field is not comparable. The concern was that the blade sections might be heavily stalled at the takeoff condition, thus precluding an accurate prediction of the propeller aerodynamics. This was not the case. Good agreement between theory and experiment is obtained at all conditions where the propeller noise exceeds the background noise.

The tunnel temperature is also measured at the beginning and end of each run. During a run the temperature changes from about 10 to 15°F. Tunnel speed is fixed by monitoring the dynamic pressure of a pitot static probe placed in the tunnel mouth and adjusting the drive fan speed. This speed is fixed to an accuracy of 0.01-in. alcohol. The rpm is monitored and the propeller motor armature and shunt field current altered to compensate for motor heating effects. In a typical run the tunnel monitor signals the propeller controller, who, in turn, tells the scope operator to capture a signal. In this way the spread in measurement conditions is minimized. The reported air speed and density are corrected for tunnel temperature drift; hence the slight variation in reported tunnel velocity during runs where the intent was to fix all parameters but one.

Theoretical Procedure

Section Characteristics

Aerodynamic characteristics of the production propeller, a flat-bottomed airfoil resembling the RAF-6 series, are calculated using a section properties algorithm implemented at Ohio State.[6] The section lift and drag properties are established at Reynolds number and Mach number corresponding to a scale model propeller turning at 10,000 rpm. Near the tip the section characteristics are calculated at velocities somewhat lower than the kinematic velocity.[4] In the aerodynamic program all section characteristics are updated using the Glauert law [Eq. (1)].

The second and third propellers have 64-series airfoil sections out to the 70% radius and 16-series airfoils from the 80% radius to the tip. A transition from one airfoil to the other occurred between the 70 and 80% radius. The section characteristics for these airfoils are from NACA TN 1546 (16 series)[7] and NACA RM L8B02 (64 series).[8] The characteristics are again corrected for each Mach number effect using Eq. (1).

Propeller Characteristics

To calculate the radial load characteristics four categories of information are needed: section characteristics, propeller shape, the influence of the nacelle, and the operating point.

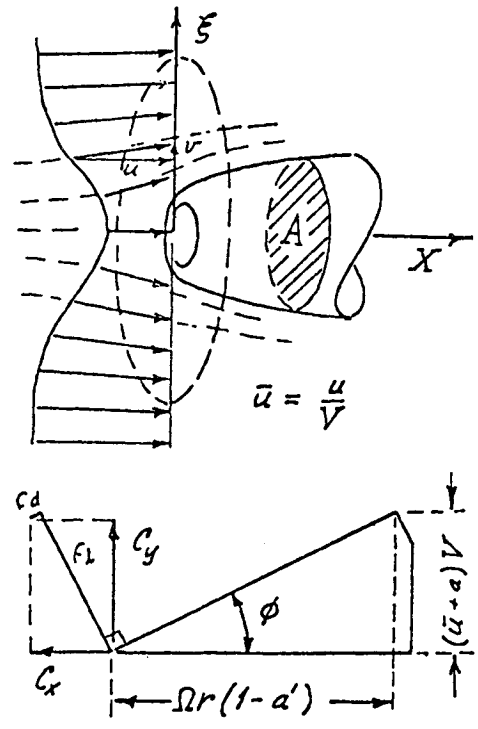

Fig. 4 Aerodynamic variables.

The selection of section characteristics is discussed in the preceding section. These characteristics are specified at ten radial stations. The propeller shape includes a description of the planform, radius, number of blades, and twist distribution. The nacelle is described by estimating the axial freestream velocity in the disk plane, which is somewhat smaller than the tunnel velocity because of blockage effect by the nacelle. The velocity field for the symmetric body is computed using the NASA LRC RAXBOL code implemented at NASA Langley. The operating point characteristics include the tunnel velocity, temperature, pressure, density, and propeller rpm. These change from run to run.

This information is used to get the radial loading by a standard lifting line technique.[1] Here an iteration scheme is used. The radial thrust loading at station r is determined in two ways: from section information and from momentum considerations (Fig. 4).

$$\frac{dT}{dr} = \frac{\rho}{2} V^2 \frac{(\bar{u}+a)^2}{\sin^2\phi} \sigma 2\pi r C_y = \rho(2\pi r) V^2 (\bar{u}+a) 2Fa \qquad (2)$$

where

p = air density
V = velocity at infinity
$V\bar{u}$ = axial velocity in disk plane as determined by the nacelle
Va = induced axial velocity at the disk plane
σ = solidity, $BC/2r$
B = number of blades
C = local chord
r = local radius
R = propeller radius
$C_y = C_l \cos\phi - C_d \sin\phi$
C_l = section lift
C_d = section drag
ϕ = angle between flow velocity and the disk plane
F = ratio of the average swirl velocity to the swirl velocity at the shed vortex sheet. F is based on the tunnel velocity V

$$= \frac{2}{\pi} \cos^{-1} \exp\left[-\frac{B\sqrt{\lambda^2+1}}{2\lambda} \left(\frac{1-r}{R} \right) \right]$$

Rearranging Eq. (2) gives

$$\frac{a}{\tilde{u}+a} = \frac{1}{4}\frac{\sigma C_y}{\sin^2\phi}\frac{1}{F} \tag{3}$$

Similar expressions for the torque give

$$\frac{1}{r}\frac{dQ}{dr} = \frac{\rho}{2}V^2\frac{(\tilde{u}^2+a)^2}{\sin^2\phi}\sigma^2\pi r C_x = \rho(2\pi r)V(\tilde{u}+a)2Fa' \tag{4}$$

where $C_x = C_l\sin\phi + C_d\cos\phi$, and Va' is the induced swirl velocity at the disk plane, which gives, using $\tan\phi = (V/\Omega r)[(\tilde{u}+a)/(1-a')]$,

$$\frac{a'}{1-a'} = \frac{1}{4}\frac{\sigma C_x}{\sin\phi\cos\phi}\frac{1}{F} \tag{5}$$

Now ϕ is equal to the twist angle β minus the angle of attack α, and is also equal to the arc tangent of the ratio of the inflow velocity to the swirl velocity

$$\phi = \tan^{-1}\left(\frac{\lambda}{\xi}\frac{\tilde{u}+a}{1-a'}\right) \tag{6}$$

where $\lambda = V/\Omega r$, $\xi = r/R$, and the angular velocity $\Omega = 2\pi n$.

To perform the calculation an inflow angle is assumed, a and a' are calculated using Eqs. (3) and (5), and ϕ is recomputed using Eq. (6). The value of ϕ is altered until the difference between successive calculations of w is small. An equivalent procedure developed by Munro[9] gives an analytic expression for the off-design loading, which avoids the need for iteration.

Acoustic Calculations

The acoustics are calculated by modeling the propeller as an array of point forces that spiral forward. These points are formed by subdividing the propeller by a series of cuts. Each point occupies the center of the section formed by such cuts, and is then assigned the net load and volume of the corresponding propeller section. Derivations of these equations are given by Succi.[2] The technique is equivalent to Farassat's methods[10] and is ultimately derived from the Ffowcs-Williams and Hawkings[11] equations.

The acoustic pressure (p) at any point in space is the sum of the contribution of the loading (p_{lk}) and thickness (p_{tk}) contribution of each of the k points.

$$p = \sum_k p_{lk} + p_{tk} \tag{7}$$

The loading noise is computed from

$$4\pi p_l = \left\{\sin(1-M_r)\left[\frac{1}{(1-M_r)^2 r^2}\frac{\hat{r}_i}{C}\frac{\partial f_i}{\partial\tau} + \left(\frac{\hat{r}_i\cdot f_i}{1-M_r}\frac{\hat{r}_i}{C}\frac{\partial M_i}{\partial\tau}\right) + \frac{1}{(1-M_r)^2 r} \times \left((\hat{r}_i f_i)\frac{1-M_i\cdot M_i}{1-M_r} - f_i M_i\right)\right]\right\} \tag{8}$$

which was first derived by Lowson.[12] Here y is the source position, x is the observer position, $M_i = [(1/c)(\partial y_i/\partial\tau)]$, $M_r = (\hat{r}_i\cdot M_i)$, $\hat{r}_i = (x_i - y_i)/r$, t is the observer time, and τ is the retarded time. Curly brackets indicate all parameters are evaluated at the retarded time $|r| = c(t-\tau)$, where c is the sound speed and f is the total force that the corresponding propeller section exerts on the air. In this paper $f_i(\tau)$ is a constant determined by the radial load calculations discussed in the preceding section.

The thickness noise is computed from[2]

$$4\pi P_t = \rho_0\left\{\sin(1-M_r) \times \frac{1}{r}\frac{1}{(1-M_r)}\frac{\partial}{\partial\tau}\frac{1}{(1-M_r)}\frac{\partial}{\partial\tau}\frac{\psi_0(\tau)}{(1-M_r)}\right\} \tag{9}$$

where $\psi_0(\tau)$ is the point volume at time τ. For propeller calculations, $\phi_0(\tau)$ is a constant determined by the corresponding propeller section volume.

In Eqs. (8) and (9) all differentiations are done analytically. No numerical solution of equations is needed. In particular, the source time for each point is incremented and both the pressure and the observer time at which the pressure is detected are calculated. A less efficient procedure is to pick an observer time, numerically calculate the retarded time for each section k along with p_{lk} and p_{tk}, then sum overall sections. Both procedures yield the same results; however, the first is computationally more efficient.

Results

Aerodynamic Results

Figures 5 and 6 compare the measured thrust and torque coefficients to the predicted values; $C_T = T/\rho n^2 D^4$, $C_p = P/\rho n^3 D^5$, where D is the thrust, P the power, n the shaft frequency, and D the propeller diameter. Here the production propeller is mounted in front of the minimum body. The low

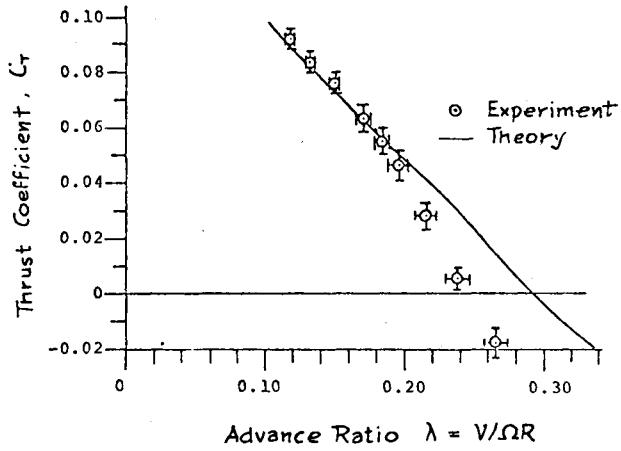

Fig. 5 Thrust coefficient vs advance ratio propeller 1, minimum body.

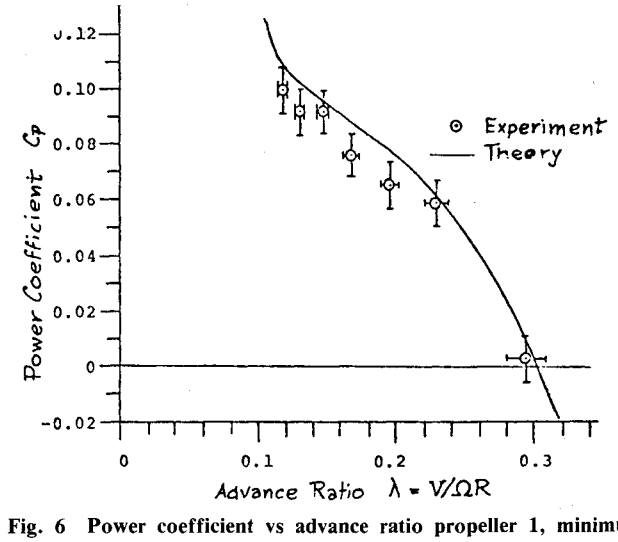

Fig. 6 Power coefficient vs advance ratio propeller 1, minimum body.

speed of the anechoic tunnel requires reduction of the propeller shaft speed for tests at high advance ratios. When the propeller speed is reduced below 7000 rpm, to attain values of λ in excess of 0.17, the experimental values of thrust and power absorption fall below the predicted values which are based on high Reynolds number airfoil characteristics. The Reynolds number at 7000 rpm for the 80% radius is 170,000 for the tunnel airspeed of 29 m/s. Assuming that zero thrust corresponds to zero lift of the outboard blade elements, the change of helix angle for zero thrust between prediction and measurement corresponds to a change in blade section lift angle of 3 deg, a not unlikely consequence of low Reynolds number. Similar discrepancies are observed with the other blades and bodies. For the most part the propeller only could be heard above the tunnel noise at rotation speeds exceeding 7000 rpm, and this deficiency did not affect the subsequent acoustic calculations.

Figures 7 and 8 are produced from the cobra probe survey of the production propeller mounted in front of the minimum body. The figures indicate the slipstream parameters infinitely far from the propeller. To develop the figures, two assumptions are made in reducing the data, which are actually taken 0.5 radii behind the propeller. First, the slipstream contracts somewhat, and all radii are assumed to correspond linearly to the percentage radii on propeller. Next, since the measurement is so close to the disk plane, the static pressure in the slipstream exceeds that of the surrounding jet. Since the theory in its original form says nothing about the axial development of the wake, all measurements are reduced to what they would be in the infinite wake. This is done in an approximate manner by assuming the energy contained in the excess static pressure appears as an increased axial velocity infinitely far behind the propeller.

Two parameters fall out of the theory: the fractional increase in axial velocity, $v_a = aV$, and the development of a tangential velocity, $v_\theta = a'\Omega R$. Figure 7 presents the axial velocity measurement and Fig. 8 presents the swirl angle $\delta = \tan^{-1}[(\Omega R/V)a'/(1+a)]$. In general, the agreement is quite good. The measured axial velocity falls somewhat below predictions near the shaft housing since the propeller was not faired smoothly into the hub. A slight dip in axial velocity is observed at the slipstream radius. This dip is caused by spurious pressure measurements near the tip vortex core.

This data reduction procedure does not work for the wake surveys made with the symmetric body. The problem is that the wake is distorted by the body. In addition, the procedure used in constructing Figs. 7 and 8 is unsatisfactory in that it references values that would be obtained in the infinite wake. The search for a proper interpretation of the wake measurements made with the symmetric body actually led to a data reduction procedure wherein measurements are compared directly to theory. The assumptions of linear contraction of the slipstream radius and development of the axial velocity from the static pressure field are unnecessary. The key to the procedure is to calculate the circulation directly, $\Gamma(p)$, and relate it to the disk plane by experimentally mapping out the line of equal mass flow. The distortion of the vortex sheets by the nacelle does nothing to alter the conservation of vortex lines. All vortex lines must originate on the vorticity bound to the blade. As the load distribution varies along its radius the vortex lines are shed into the flow. This circulation, Γ, is $2\pi r_p \langle v_\theta \rangle_p$, where r_p is the measurement radius and $\langle v_\theta \rangle_p$ the time average of the azimuthal velocity at the measurement point p. Thus, by doing a wake survey at all values r_p from the nacelle to beyond the slipstream, the circulation $\Gamma(p)$ can be mapped as a function of radius. Since $\Gamma(p)$ is also equal to the circulation around the blade, this gives a measure of the blade loading.

The next task is to relate r_p to the corresponding point on the blade. This difficulty may be overcome by noticing that the incompressibility of the flow guarantees that the mass flow at a given radius can change only if the axial velocity changes in a compensating way. Mapping out lines of equal mass flow in effect maps out the stream surfaces. If one assumes the propeller is lightly loaded and the flow is inviscid, then the shed vortex lines follow the unperturbed stream surfaces; that is, the stream surfaces that would exist in the absence of a propeller.

The mass flow at any radius is calculated from the theoretical axial velocity $(\bar{u}+a)V$ at all radii in the disk plane. If the probe starts at the propeller tip and integrates the mass flux as it moves to the hub, each value of the mass flow corresponds in a one-to-one fashion to a particular value of the circulation. Thus the tabulation of $\langle v_\theta \rangle_p$ and $\langle v_a \rangle_p$ at some axial distance downstream allows one to reconstruct the circulation on the blade.

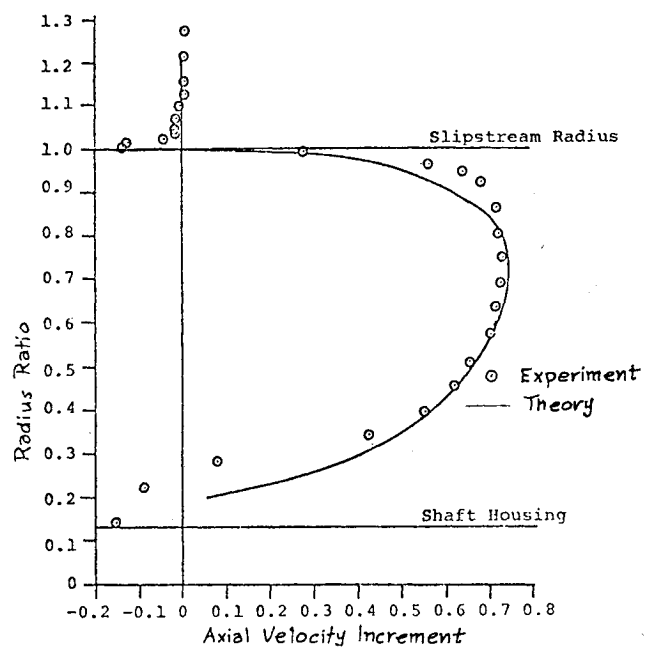

Fig. 7 Axial velocity increment in the infinite wake: propeller 1, minimum body, 10,000 rpm, 29 m/s.

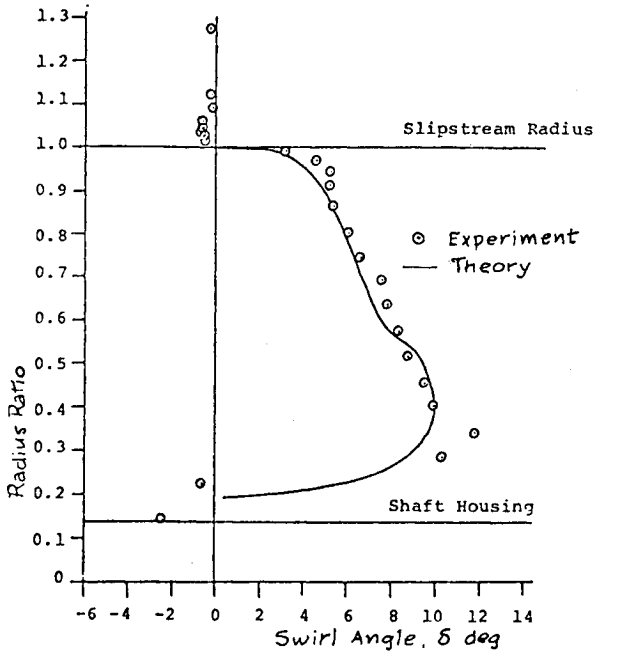

Fig. 8 Swirl angle in the infinite wake: propeller 1, minimum body, 10,000 rpm, 29 m/s.

Figure 9 presents the results of just such a calculation for the production propeller mounted in front of the symmetric body. Measurements are taken one-half radius downstream from the disk plane, and are deduced from the hot wire data. The equivalent radius is the square root of the measured mass flow normalized to unity at the slipstream boundary. In uniform flow the radius of a cylinder is directly proportional to the square root of the mass flow. Hence this method of plotting does not weigh the tip region so heavily as would be the case if mass flow was the horizontal axis. Again the calculation gives an accurate estimate of the radial load distribution.

Figure 10 is a plot of circulation vs mass flow for the production propeller in front of the minimum body, just as in Figs. 7 and 8. Now, however, the probe is a hot wire velocimeter and the data reduction procedure is more direct. Again good agreement is obtained between theory and experiment.

Figure 11 is a plot of circulation vs mass flow for propeller 3 operating in front of the minimum body. As before, the theory and calculations agree. Hence the measurement is made 3 cm (0.12 radii) behind the disk plane. An interesting feature is the shape of the circulation curve. Even in this off-design condition the loading is moved significantly inboard.

Comparison of Figs. 10 and 11 reveals that the tip loading of both propellers is nearly the same. However, the inboard loading of propeller 3 exceeds that of the production propeller. Aerodynamically, this means that its power absorption is somewhat greater. Acoustically, this means that its pressure signature is also somewhat greater. Thus, when acoustic comparisons are made between the two, based on the off-design tests, no acoustic benefits result. This is not a deficiency in the theory that describes the propeller characteristics' on or off design. In fact, the close agreement between measurements and predictions at the off-design condition is a strong indication that the theory accurately describes the design condition. Subsequent calculations showed that the off-design performance of propeller 3 can be made to match that of the production propeller and still maintain the acoustically beneficial inboard loading at the design condition. This fine tuning is accomplished by modifications to the tip and twist distribution.

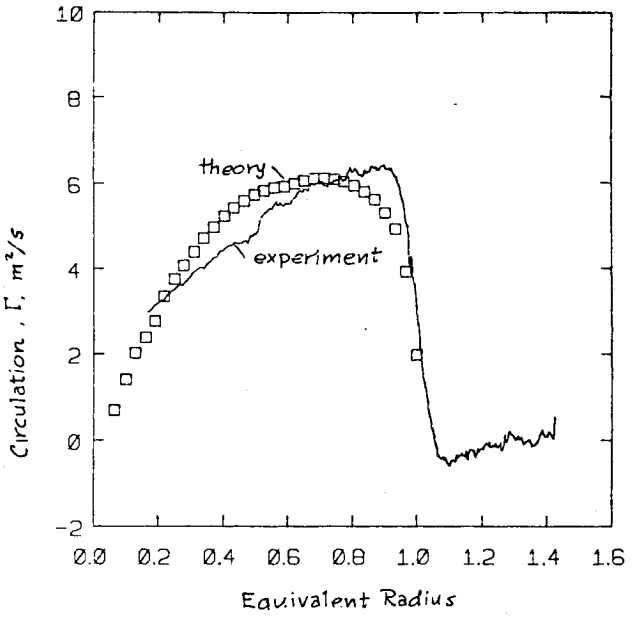

Fig. 9 Circulation vs equivalent radius: propeller 1, symmetric body, 10,000 rpm, 29 m/s.

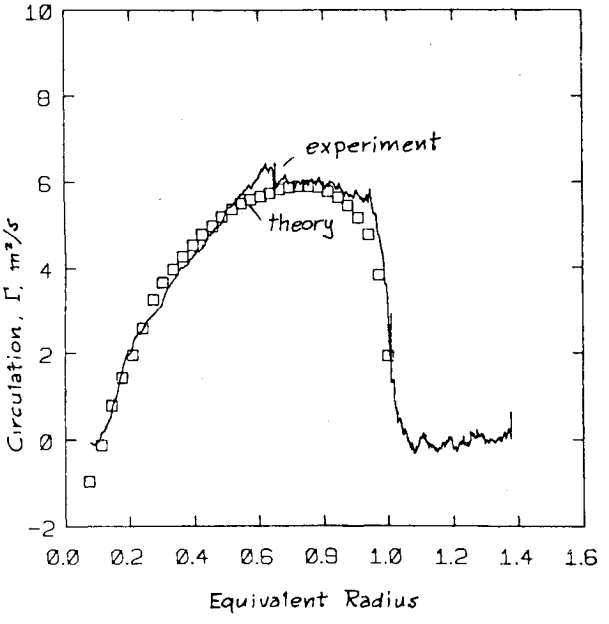

Fig. 10 Circulation vs equivalent radius: propeller 1, minimum body, 10,000 rpm, 29 m/s.

Acoustic Results

The acoustic theory applies only to the periodic component of propeller noise, which is sometimes called rotational noise. In order to compare the experimental results it is first necessary to extract the best possible estimate for the part of the sound that has the same period as the blade passages. To do this, the raw signal, composed of several pressure pulses, is Fourier transformed. The average signal is produced by inverse transforming the first of 64 harmonics of the blade passing frequency. In addition, some effort is made to mitigate the effect of the 30-Hz high pass filter, which is used to minimize the low frequency background noise. The filter causes a phase shift in the first few harmonics of the blade passage. Since the frequency components are extracted, it is quite simple to allow for the effect of the filter. So, it is the unfiltered periodic part of the signal that is compared to the predictions. This procedure and other test cases are discussed at length by Munro.[9]

To assure the reader that the information is not distorted in the process, Fig. 12 is included. Here the theoretical calculations are compared to several cycles of the raw data taken from the production propeller in front of the symmetric body (unless specifically stated all other references are made to this propeller body combination). It is quite clear that there are differences from cycle to cycle. In particular the second, fourth, and sixth pressure spikes are all greater than the preceding spike. What one observes is the result of small manufacturing differences between the two blades. In addition there is a fluctuation about the mean signatures that is not background tunnel noise. The task, however, is to calculate the periodic portion of the signature. From the figure it is evident that calculation agrees well and greater data reduction efforts are needed to make a more stringent test of the theory. The theory is adjusted neither in amplitude nor phase. The only processing of the theoretical calculations is to subtract off the steady near-field pressure that the microphone cannot detect.

Figure 13 is the same condition as Fig. 11; however, the data are processed to extract the periodic part. Here and in subsequent graphs zero time corresponds to a source time at which the propeller is vertical. The several traces are samples of the same data taken at different times and indicate the repeatability of the measurement. About nine months separate the first measurement from the last. Some differences are expected since the tunnel temperature and propeller rpm were not the same at the instant the waveforms were collected. A more subtle effect is that the number of

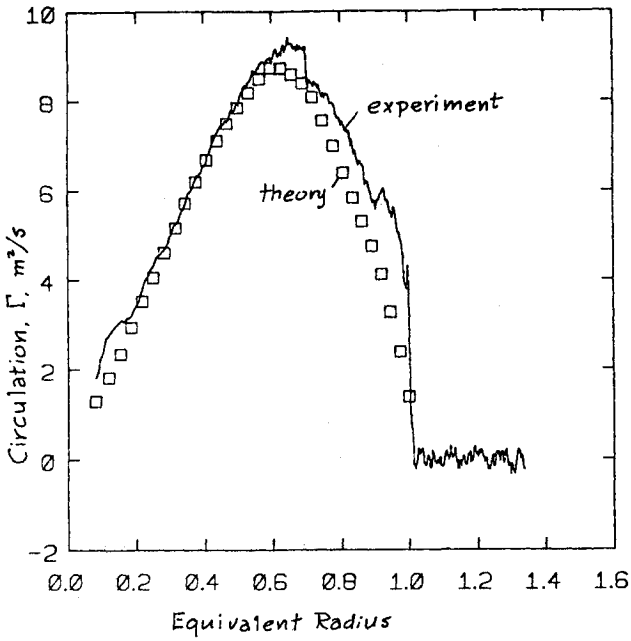

Fig. 11 Circulation vs equivalent radius: propeller 3, minimum body, 10,000 rpm, 29 m/s.

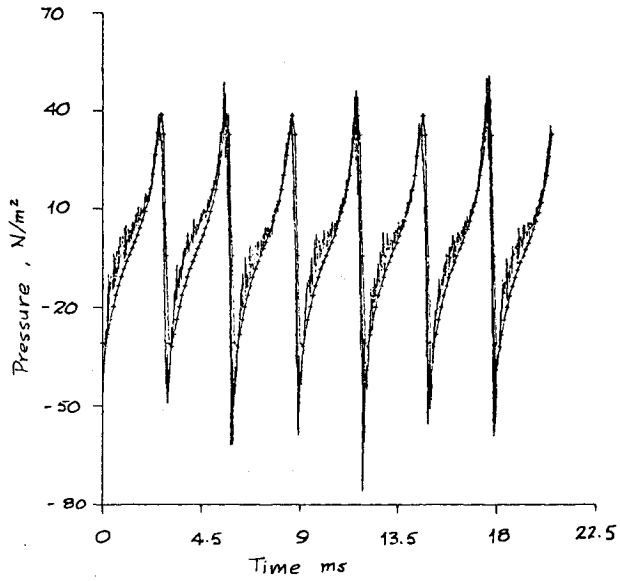

Fig. 12 Comparison of predictions to unprocessed measured pressure signature: propeller 1, symmetric body, 10,000 rpm, 29 m/s, 0-deg azimuth.

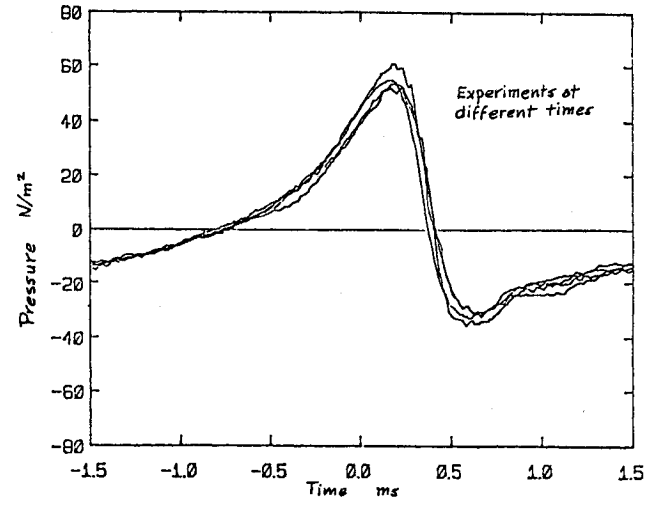

Fig. 13 Repeatability of the measured pressure signature: propeller 1, symmetric body, 10,000 rpm, 29 m/s, 10-deg azimuth.

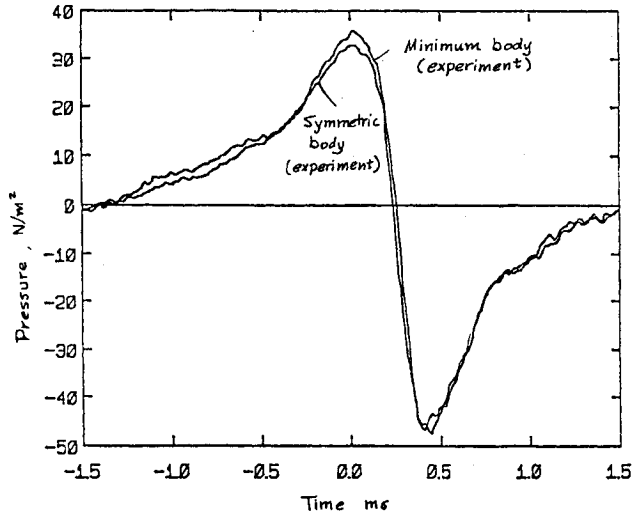

Fig. 14 Comparison of measured pressure signature between the minimum and symmetric body: propeller 1, 10,000 rpm, 29 m/s, 0-deg azimuth.

blade passages that were averaged in order to obtain the plot is different in each case. Calculations show that these differences can be explained on the basis of the measured differences between temperature and rpm from case to case.

Figure 14 compares the disk plane pressure signature of the production propeller mounted in front of the minimum and symmetric bodies. The signatures are identical. Inspection of the wake surveys[5] revealed that the tip loading is also nearly identical; hence the similarity in pressure signatures. There is some evidence that differences appear at higher advance ratios, but these are difficult to state accurately because of tunnel speed limitations. To get the higher advance ratio the tip speed is dropped to 7000 rpm and the signal-to-signal noise ratio is decreased. Moreover, there is no noticeable difference between the symmetric and asymmetric tests. Henceforth, discussion is retricted to propellers operating in front of the symmetric body.

Figures 15-17 compare the calculated and measured signatures at several azimuths. Here +40 deg places the observer in front of the propeller, 0 deg in the disk plane, and −40 deg puts the observer behind the propeller. The changes in shape of the waveform agree well with predictions over the entire range of microphone azimuths. The measured sound leads the predicted sound slightly behind the disk plane while lagging it slightly ahead of the disk plane. There also appears to be a tendency to underpredict the sound behind the disk plane and overpredict it ahead of the disk plane. These differences could be the result of the neglect of sound produced by the rollup of the vortex wake, inaccuracies in the predicted loads, or perturbations on the sound field by the test section.

Note that the sound directivity pattern is distorted by the proximity of the microphone to the propeller. In the acoustic far field, the signature at all azimuths resembles the disk plane signature in shape. That the acoustic theory reproduces the pressure field this close to the propeller is a strong test of its accuracy.

Figure 18 indicates the results of decreasing the propeller speed at constant advance ratio and should be compared to Fig. 16. Here the microphone is in the disk plane. Only the Mach numbers of the blade section are altered in this process; attack angles remain substantially unchanged. The decrease in

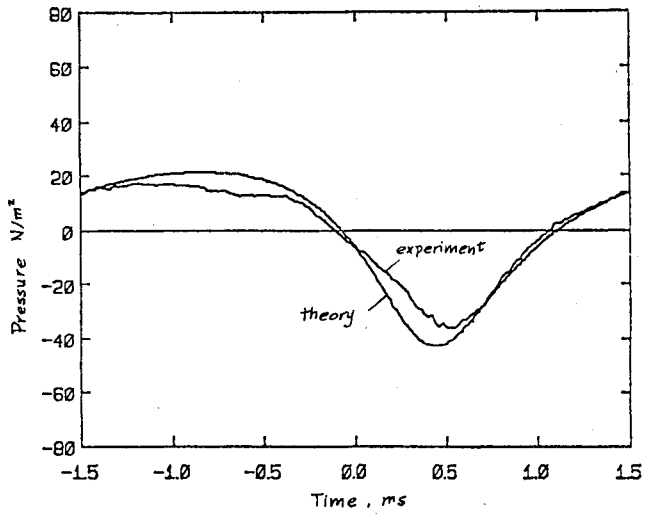

Fig. 15 Comparison of measured and predicted pressure signature: propeller 1, symmetric body, 10,000 rpm, +40-deg azimuth.

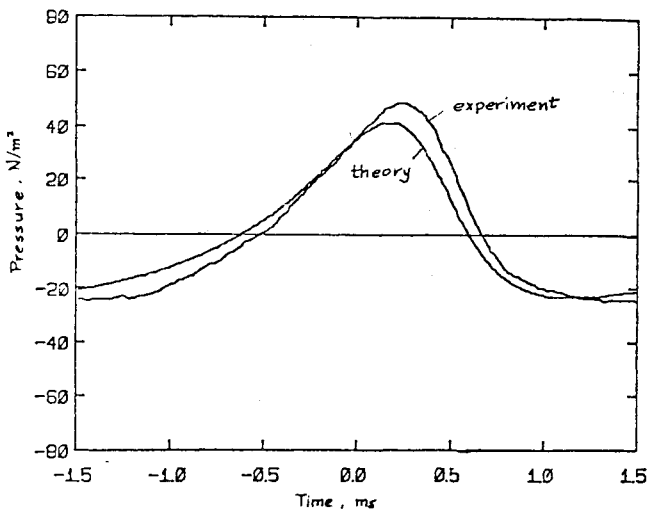

Fig. 17 Comparison of measured and predicted pressure signature: propeller 1, symmetric body, 10,000 rpm, −40-deg azimuth.

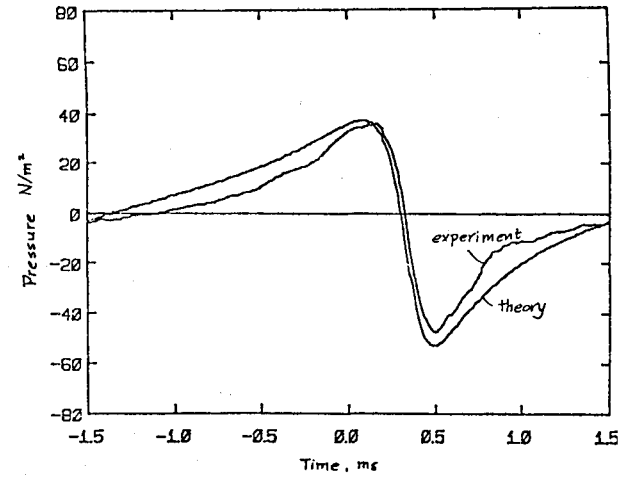

Fig. 16 Comparison of measured and predicted pressure signature: propeller 1, symmetric body, 10,000 rpm, 0-deg azimuth.

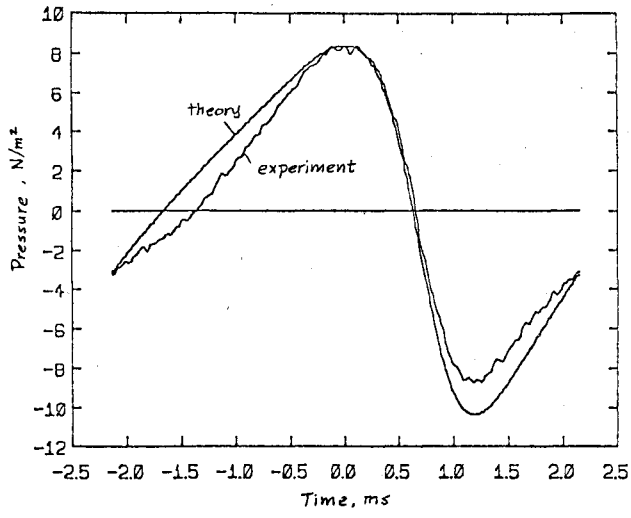

Fig. 18 Comparison of measured and predicted pressure signature: propeller 1, symmetric body, 7000 rpm, 20 m/s, 0-deg azimuth.

sound amplitude at low Mach numbers is partly due to decreased loading and partially to decreased Mach number. Again the theory captures the effect.

Figure 19 indicates the results of decreasing the propeller speed at constant tunnel velocity. Here the most interesting comparison is to Fig. 18, which is at the same rpm. As the blade element Mach number is determined primarily by the rotation rate, these tests are the same except for load variations. Figure 19 is at a substantially greater advance ratio and the propeller is therefore less loaded. This load change manifests itself as a reduced amplitude of the signature; here the zero-to-peak amplitude drops from 8½ to 7 P. Again the differences are captured quite accurately by the theory.

Figure 20 is an example of propeller 3 mounted in front of the symmetric body. The operating condition is 10,000 rpm and 29 m/s tunnel velocity. The microphone is held in the disk plane. Here we find a phase differential between theory and experiment. This shift, however, is entirely due to calibration errors in the optical trigger. Late in the project it was discovered that the optical trigger had a phase shift that varied slightly with rpm.[9] It was possible to back calibrate all the runs except for a few; this happens to be one.

Figure 21 is an example of propeller 2 operating under the same conditions as in Fig. 20. Notice that the amplitude of the sound is considerably greater than for the other two blades, a fact that follows from the greater loading and power absorption. In contrast to the production blade the theory noticeably underpredicts the peak-to-peak amplitude of the fluctuations in the disk plane. This may be due to the low values assumed for the profile drag coefficients of the airfoil section. These same low drag coefficients were used for propeller 3, which has identical airfoil sections. Close inspection of Fig. 20 shows the sound pressure was underpredicted in that case as well. However, the effect vanishes for both propellers at 7000 rpm and again theory and calculation agree.

Further notice the possible shock steepening seen in recovery of the pressure from its negative excursion. This effect is more pronounced for propeller 2 than it was for either of the others, which are more lightly loaded. A nonlinear effect would have just this characteristic; it should be more pronounced for large amplitude disturbances. This is the first indication in these experiments that the linear theory breaks down. Hence care must be taken if these techniques are applied to propellers with greater disk loading, which increases the sound amplitude. Higher tip speeds have a similar effect.

Extensive comparisons have also been made for the predicted and measured frequency spectra of several full-scale

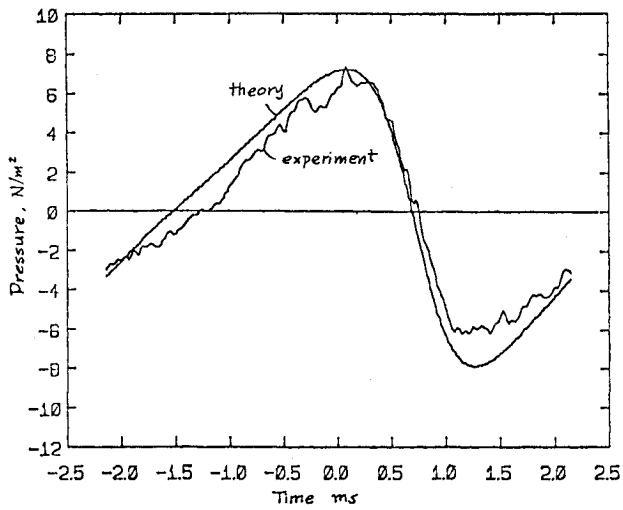

Fig. 19 Comparison of measured and predicted pressure signature: propeller 1, symmetric body, 7000 rpm, 29 m/s, 0-deg azimuth.

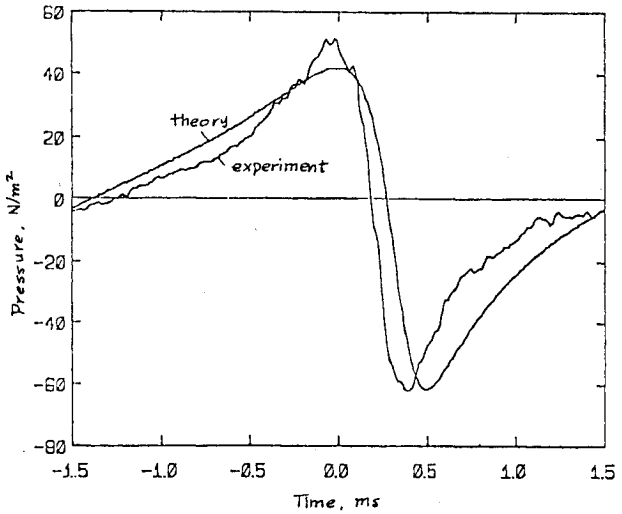

Fig. 20 Comparison of measured and predicted pressure signature: propeller 3, symmetric body, 10,000 rpm, 29 m/s, 0-deg azimuth.

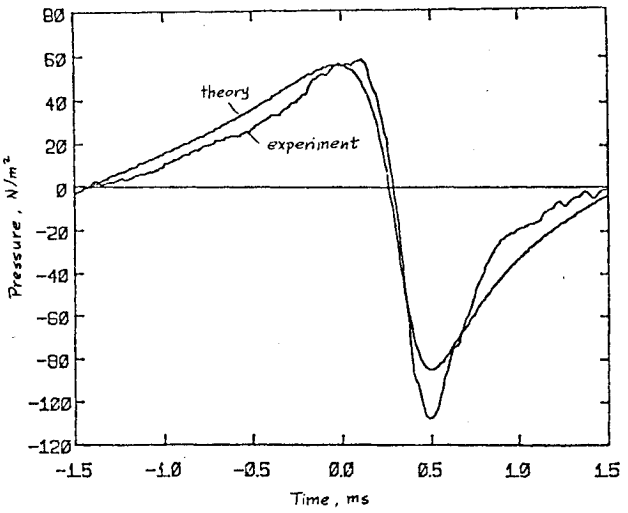

Fig. 21 Comparison of measured and predicted pressure signature: propeller 2, symmetric body, 10,000 rpm, 29 m/s, 0-deg azimuth.

propellers. These comparisons may be found in Refs. 10, 13, and 14. The same techniques described in this paper are used for the predictions. Similar accuracy is obtained. For spectral comparisons, the amplitude between predicted and measured spectra is obtained up to the point where the spectal lines are buried in the instrument noise. For sufficiently high speed propellers nearly 20 harmonics are observed with little or no discrepancy between theory and measurements.

Summary

One can predict the sound from a propeller given only its shape and motion; no adjustable constants are needed. To do this, first the blade load distribution is calculated, then the sound field is calculated.

Experiments are carried out that validate the aerodynamic and acoustic calculations. The aerodynamic experiments verify both the net thrust and torque predictions and also the radial distribution of the loads. A more important result is the close agreement between the measured and predicted acoustic pressure signatures. The difference caused by changing propellers, propeller operating conditions, and observer location are all accurately described by the theory.

Acknowledgment

This research was supported by NASA-15154 granted from NASA Langley Research Center and cosponsored by the EPA.

References

[1] Larrabee, E. E., "Practical Design of Minimum Induced Loss Propellers," Paper 790585, *SAE Transactions*, SAE, Warrendale, Pa., April 1979.

[2] Succi, G. P., "Design of Quiet Efficient Propellers," Paper 790585, *SAE Transactions*, SAE, Warrendale, Pa., April 1979.

[3] Bauer, P. and Widnall, S. E., "The Development of a Wind Tunnel Facility for the Study of V/STOL Noise," Flight Transportation Lab. Rept. FTL R-72-6, MIT, Cambridge, Mass., 1972.

[4] Dunbeck, P. B., "Performance of Light Aircraft Propellers," S.M. thesis, MIT Dept. of Mechanical Engineering, Cambridge, Mass., Feb. 1979.

[5] Zimmer, J., "Wakes and Performance of Light Aircraft Propellers," S.M. thesis, MIT Dept. of Mechanical Engineering, Cambridge, Mass., June 1980.

[6] Korchan, K. D., Beall, B. W., and Gregorek, G. M., "Two-Dimensional Aerodynamic Analyses of Nine Propeller Sections," GA/ADAC TDR 78-04, Oct. 1978.

[7] Lindsay, W. J., Stevenson, D. B., and Daley, B. D., "Aerodynamic Characteristics of 24 NACA 16 Series Airfoils," NACA TN 1546, 1948.

[8] Kaften, L. K. and Poteat, M. J., "Aerodynamic Characteristics of Several NACA Airfoil Sections at Seven Reynolds Number from $0.7 \cdot 10^6$ to $9 \cdot 10^6$," NACA RM L8B02, May 1948.

[9] Munro, D. H., "The Production of Sound by Moving Objects," Ph.D. thesis, MIT Dept. of Physics, Cambridge, Mass., June 1980.

[10] Farassat, F. and Succi, G. P., "A Review of Noise Prediction Technology with Emphasis on Two Current Methods for Time Domain Calculations," *Journal of Sound and Vibration*, Vol. 71, No. 3, Aug. 8, 1980.

[11] Ffowcs-Williams, J. E. and Hawkings, D. J., "Sound Generated by Turbulence and Surfaces in Arbitrary Motion," *Philosophical Transactions of the Royal Society (London)*, A264, 1969.

[12] Lowson, M., V., "The Sound Field of Singularities in Motion," *Proceedings of the Royal Society (London)*, A286, 1965.

[13] Succi, G. P., "Computed and Experimental Spectra for a Wing-Mounted Microphone on a Light STOL Aircraft," NASA CR 165725, May 1978.

[14] Succi, G. P., "On the Design and Test of a Low Noise Propeller," BBN Rept. No. 4764, Aug. 1981.